Applications of Micro-CT scanning in medicine and dentistry: Microstructural analyses of a Wistar Rat mandible and a urinary tract stone

F D E Latief[1]*, D S Sari[2] and L A Fitri[3]
[1]Physics of Earth and Complex Systems, Faculty of Mathematics and Natural Sciences, Institut Teknologi Bandung, Bandung, Indonesia
[2]Department of Periodontology, Faculty of Dentistry, Universitas Jember, Jember, Indonesia
[3]Biophysics, Faculty of Mathematics and Natural Sciences, Institut Teknologi Bandung, Bandung, Indonesia

*E-mail : fourier@fi.itb.ac.id

Abstract. High-resolution tomographic imaging by means of x-ray micro-computed tomography (μCT) has been widely utilized for morphological evaluations in dentistry and medicine. The use of μCT follows a standard procedure: image acquisition, reconstruction, processing, evaluation using image analysis, and reporting of results. This paper discusses methods of μCT using a specific scanning device, the Bruker SkyScan 1173 High Energy Micro-CT. We present a description of the general workflow, information on terminology for the measured parameters and corresponding units, and further analyses that can potentially be conducted with this technology. Brief qualitative and quantitative analyses, including basic image processing (VOI selection and thresholding) and measurement of several morphometrical variables (total VOI volume, object volume, percentage of total volume, total VOI surface, object surface, object surface/volume ratio, object surface density, structure thickness, structure separation, total porosity) were conducted on two samples, the mandible of a wistar rat and a urinary tract stone, to illustrate the abilities of this device and its accompanying software package. The results of these analyses for both samples are reported, along with a discussion of the types of analyses that are possible using digital images obtained with a μCT scanning device, paying particular attention to non-diagnostic *ex vivo* research applications.

1. Introduction

Imaging techniques such as scanning electron microscopy (SEM), magnetic resonance imaging (MRI), ultrasonography, x-ray radiography, and x-ray computed tomography (CT) have played a significant role in the development of many life science–related fields, including medicine and dentistry. Many of these imaging modalities, e.g. MRI and CT, have the ability to produce 3-D images of the object(s) of interest. The x-ray medical CT uses the concept of digitizing x-ray attenuation which is captured by the detectors. In this system, the source and the detectors are rotating around the object in a minimum of 180° rotation in which the recorded sinograms are then reconstructed by means of an inversion technique to obtain a 3D visual of the object.

Imaging techniques are utilized for both diagnostic and non-diagnostic imaging. in the U.S., for diagnostic purposes, including use in clinical research for patient diagnoses, the technique as well as the corresponding hardware and software needs to be approved by the Food and Drug Administration (FDA); for non-diagnostic (pre-clinical) research, such approval is not necessary. One widely used

technique in the pre-clinical research is x-ray micro–computed tomography (μCT). Although μCT is largely the same as x-ray medical CT, μCT allows the observation of more detailed structures of a sample, on the order of micrometers. μCT also has a different way of obtaining projection images, i.e., in μCT, the positions of the source and the detector are fixed, and the sample rotates.

In this study, we analyzed the application of a μCT scanning device, the Bruker SkyScan 1173. One of the key features of this device is that its x-ray energy source ranges from 40 kV (although it is possible to adjust the source energy from 20 kV) to 130 kV. This range allows the SkyScan to be applied to a wide variety of research cases, in both the material and life sciences. It has been utilized in many types of dental [1-6] and general medicine [7-11] applications. This particular device, which is installed in a research facility belonging to the Faculty of Mathematics and Natural Science at Indonesia's Institut Teknologi Bandung, has been used in many researches in the field of medicine [12-16] and material sciences [17-21].

This paper presents our analyses of two samples related to life sciences using SkyScan 1173. General workflows as well as several measurable characteristics are described to provide a depiction of the commonly utilized features and abilities of this technique. This paper will also present the standard terminology or nomenclature and units used, which should be included when describing the utilized methods (primarily for *ex vivo* evaluations), as well as the results of our analyses.

2. Materials and Methods

In this study, two samples were used: a mandible from a wistar rat and a urinary tract stone, shown in Figures 1(a) and 1(b). The samples were scanned using a Bruker SkyScan 1173 (see Figure 1(c). As discussed above, this device has a wide range of potential x-ray energy output levels (40-130 kV), making it possible to scan both soft tissues and hard, high-density materials such as stone and metals.

The device produces microstructural 3-D images of a sample by means of x-ray attenuation; these images are recorded by a flat panel detector. The SkyScan 1173 system mainly consists of an x-ray source, a rotating object stage/holder, and a flat panel detector and converter system, which converts the attenuated analogue signal into a digital image. The scanning process requires the sample to be rotated a minimum of 180°. The degree of rotation is adjusted according to the preferred image resolution. The SkyScan 1173 can generate three different image quality levels: standard (spatial resolution of 20 to 140 μm), medium (10 to 70 μm) and high (5 to 35 μm). A good contrast ratio between the scanned components and amount of noise (sometimes referred as the high signal-to-noise ratio) in the produced image can be obtained by fine-tuning the scanning parameters. The scanning parameters for this study are listed in Table 1.

(a)

(b)

(c)

Figure 1. (a) wistar rat mandible, (b) urinary tract stone, and (c) SkyScan 1173 μCT scanning device

Table 1. Scanning parameters for the wistar rat mandible and urinary tract stone

Parameter	Value	
	Mandible	***Stone***
energy [kV]	80	80
current [μA]	50	100
exposure time [ms]	125	1000
filter type	-	Al 1.0 mm
rotation step	0.2	0.2
camera binning	4×4	1×1
dimension of projection image	560×560	2240×2240
raw image resolution [μm/pixel]	24.23	14.96
frame averaging	10	10

From the scanning process, a series of projection images similar to those obtained via x-rays were produced. The 3-D structure of the sample can be determined by reconstruction of the projection images using NRecon software, which employs the Feldkamp backprojection algorithm. A Graphical Processing Unit (GPU)-based kernel reconstruction using GPUReconServer is recommended over the conventional Central Processing Unit (CPU)-based kernel reconstruction using NReconServer due to its ability to accelerate the reconstruction using GPU cores. GPU processing cores are generally faster for exhaustive numerical process compared to CPU processing. During the reconstruction, some visible artefacts can be reduced by means of post-alignment compensation, which corrects misalignment of the projection images caused by movement of the sample during scanning; ring artifact reduction, a process for reducing artifacts that appear as circular patterns resulting from rotation of the sample; and beam hardening correction, which rebalances the significantly lower grayscale at the center of an image of a dense object compared to its outer edges.

During the reconstruction process, the voxel size of the reconstructed image can be customized (downscaled) if necessary. The reconstructed image has lower resolution (high voxel size) compared to the projection images. This option reduces the dataset size, but also reduces the accuracy and level of detail in the reconstructed images, thus this option should be used only when necessary. For example, medium- to low-resolution 3-D images are adequate for qualitative analyses consisting of simple visual identification of homogeneous samples.

In reconstruction, a greyscale 3-D image is created from a series trans-axial (sliced along the *z* axis, or *x*-*y* plane) 2-D images. The grayscale level is related to the density of the sample. Denser parts of the sample show up as bright areas in images, while lower density is indicated by darker areas.

The SkyScan 1173 device comes with a bundle of image processing and analysis software, in addition to the control (SkyScan1173) and reconstruction software (NRecon). One such program, DataViewer, allows for qualitative analyses to be done by visual inspection of 2-D images, including sagittal (sliced on the *x* axis, or *z*-*y* plane) and coronal (sliced on the *y* axis, or *x*-*z* plane) images, in addition to the trans-axial images mentioned above. DataViewer is also capable of visualizing these three cross-sectional planes as orthogonal slices (ortho-slice). Image contrast and window-level adjustment can be done with DataViewer, as well as image rotation (on the *x, y,* and *z* planes), color-coding, box-shaped cropping (VOI selection), and image registration in 2-D and 3-D.

Three-dimensional volume rendering can be conducted using the CTVox software, in which several 3-D manipulations can be done without altering the original dataset. Rotation in 3-D, object slicing, and cropping are some of the basic features of CTVox, allowing for inspection of the interior structure of the sample. Adjustment of opacity and luminosity, key to inspection and isolation of sample composition and density, are also possible, as is colorization of the sample, which can be done by adjusting the histogram of Red-Green-Blue (RGB) values.

2.1. General Workflow of Analysis and Measured Parameters

μCT imaging techniques facilitate examination of a sample without destroying it via image processing and analysis. Prior to a typical image analysis, there are two basic image processing procedures that need to be conducted. First is the definition of a region of interest (ROI), or a volume of interest (VOI) for 3-D images, inside which analyses will be localized. Then segmentation must be done by applying a threshold value of the grey-level to the sample. This is very important in defining which component(s) of the sample is of interest in the analysis, and which part(s) should be omitted. Various objective (automated) thresholding methods are widely available, accessible through software such as CTAnalyzer (CTAn). The two main thresholding methods in CTAn are the global histogram-based method (automatic Otsu in 2-D and 3-D), and the local one (adaptive threshold).

After defining the ROI/VOI and thresholding, other processing and analysis can be done as necessary on a case-by-case basis. CTAn provides various image processing functions such as filtering (including smoothing, noise reduction and unsharping), morphological operations (e.g. erosion, dilation, opening, closing, watershed operation), despeckling (speckle removal), ROI shrink-wrap (shrink the ROI to the boundaries of a binarized object), bitwise operations (binary arithmetic operations), arithmetical operations, and geometrical transformation (e.g. flip, rotate, translate). After any necessary image processing, measurements can be taken. Table 2 shows the typical morphometric parameters that can be calculated using CTAn. The nomenclature based on the American Society for Bone and Mineral Research (Bone ASBMR) is based on [22]. Other parameters can also be measured when necessary by means of direct calculations/operations featured in CTAn, or by doing further calculations using the measurements of the various parameters.

Table 2. Typical morphometric parameters for life science–related samples

Parameter Name; Symbol; and Unit		**Brief Description**
General Scientific	***Bone ASBMR***	
total VOI volume; TV; mm^3	tissue volume; TV; mm^3	total volume of the volume of interest (VOI), based on the marching cubes volume model
object volume; Obj.V; mm^3	bone volume; BV; mm^3	total volume of binarized objects within the VOI, based on the marching cubes volume model
percent object volume; Obj.V/TV; %	percent bone volume; BV/TV; %	proportion of the VOI occupied by binarized solid objects
total VOI surface; TS; mm^2	tissue surface; TS; mm^2	surface area of the VOI, measured in 3-D, based on the marching cubes method
object surface; Obj.S; mm^2	bone surface; BS; mm^2	surface area of all the solid objects within the VOI, measured in 3-D, based on the marching cubes method
object surface/ volume ratio; Obj.S/Obj.V; mm^{-1}	bone surface/ volume ratio; BS/BV; mm^{-1}	ratio of solid surface to volume measured within the VOI, often referred as “specific surface area,” commonly used in characterizing the complexity of structures
object surface density; Obj.S/TV; mm-1	bone surface density; BS/TV; mm-1	ratio of surface area to total VOI volume
structure thickness; St.Th; mm	trabecular thickness; Tb.Th; mm	measurement of the solid structure’s thickness where the thickness of a given local point in the sample is defined by [23]; the key advantage of the local thickness measurement is defined by [24]; and the distance transform method is defined by [25]
structure separation; St.Sp; mm	trabecular separation; Tb.Sp; mm	measurement of the spaces as defined by binarization within the VOI, employing the same method used for measuring trabecular thickness, but applied to the empty space rather than the solid voxels
total porosity; Po(tot); %	total porosity; Po(tot); %	pore volume as a percentage of total VOI volume

3. Results and Discussion

The scanning process produces a series of raw projection images in 16-bit TIFF file format. Previews of the images from this study can be seen in Figure 2. The interior microstructure of the sample, however, cannot be determined using only these images. From the previews, Figure 2(a) appeared brighter than Figure 2(b). This seemed to indicate that Sample 2 was composed of higher-density

materials than Sample 1. To verify this initial impression, though, reconstruction and further (qualitative and quantitative) analyses must be done.

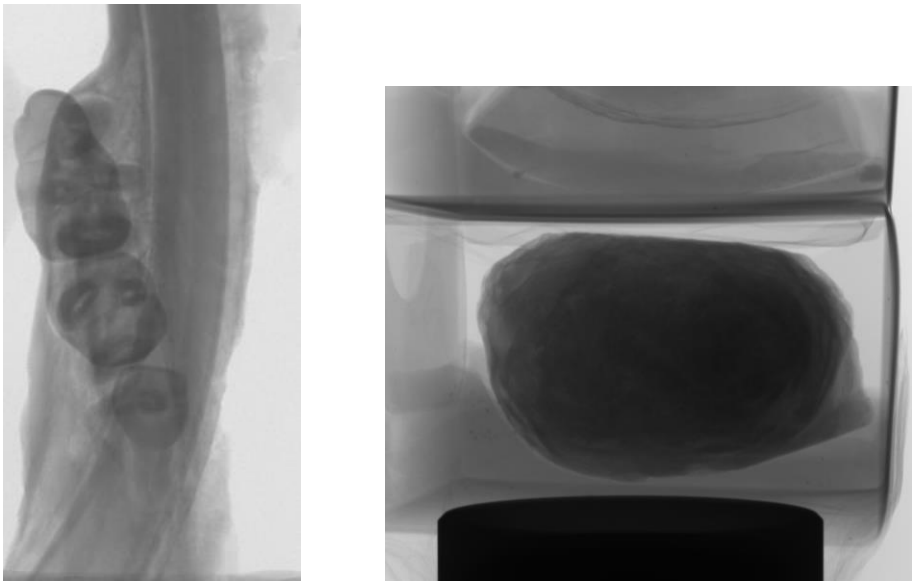

(a) (b)

Figure 2. Previews of projection images for the (a) wistar rat mandible and (b) urinary tract stone

Figure 3 shows the results from the reconstruction process, visualized by DataViewer in trans-axial, coronal, sagittal and ortho-slice images. The data produced from the reconstruction process are shown in 8-bit BMP (grayscale) images: the wistar rat mandible in Figure 3, and the urinary tract stone in Figure 4. The grayscale level shows the relative density of the materials that comprise the sample: brighter areas indicate higher density and vice versa. In Figure 3, high-density objects such as dental crowns appear as brighter areas; some brighter spots are also visible in Figure 4, indicating that the stone is heterogeneous in composition. Three-dimensional volume renderings (generated using CTVox), used for visual inspection, are shown in Figure 5. Figures 5(c) and 5(d) were sliced to show the interior structures of the samples.

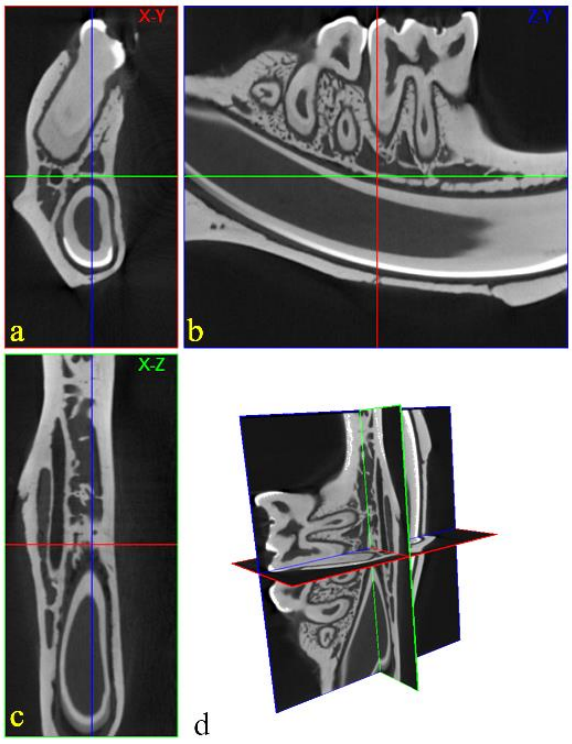

Figure 3. Reconstructed images of the wistar rat mandible: (a) trans-axial slice; (b) sagittal slice; (c) coronal slice; (d) ortho-slice

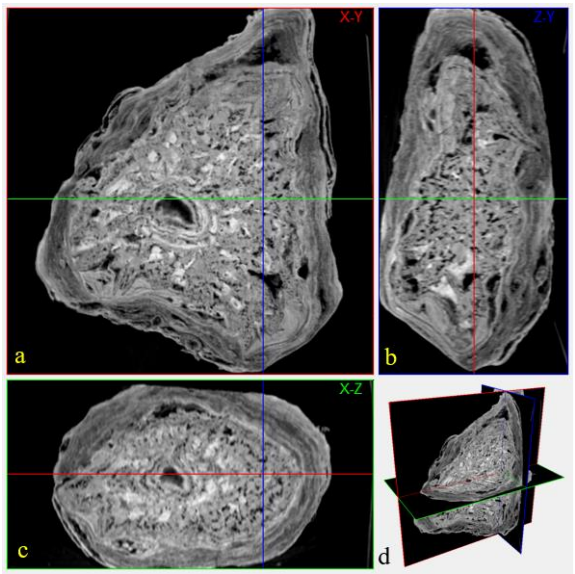

Figure 4. Reconstructed images of the urinary tract stone: (a) trans-axial slice; (b) sagittal slice; (c) coronal slice; (d) ortho-slice

Following visual inspection (as part of qualitative analysis), appropriate VOIs were selected and suitable thresholds were applied prior to quantitative analysis. VOI selection was done using the ROI shrink-wrap feature in CTAn, allowing for the generation of an irregular VOI corresponding to the outer shape of the sample. This method uses a binary image of the sample to shrink the ROI and wrap around the shape of the sample; it is possible to use this method in both 2-D and 3-D space. Afterwards, an automatic threshold based on the global 2-D Otsu method was applied to both samples.

3.1. Measured Parameters

Parameters listed in Table 2 were measured for both samples; Table 3 presents these measurements. Another measured parameter for the molar sample is the distance between the cementoenamel junction (CEJ) and the procesus alveolar. By measuring this distance, conditions such as bone resorption can be analyzed. For Sample 1, this distance can be measured using CTAn by drawing a line from the CEJ to the procesus alveolar on a given slice, as shown in Figure 6. In Sample 2, additional analyses (such as determination of the sample's chemical composition) can also be conducted (reported in detail in [16, 17]).

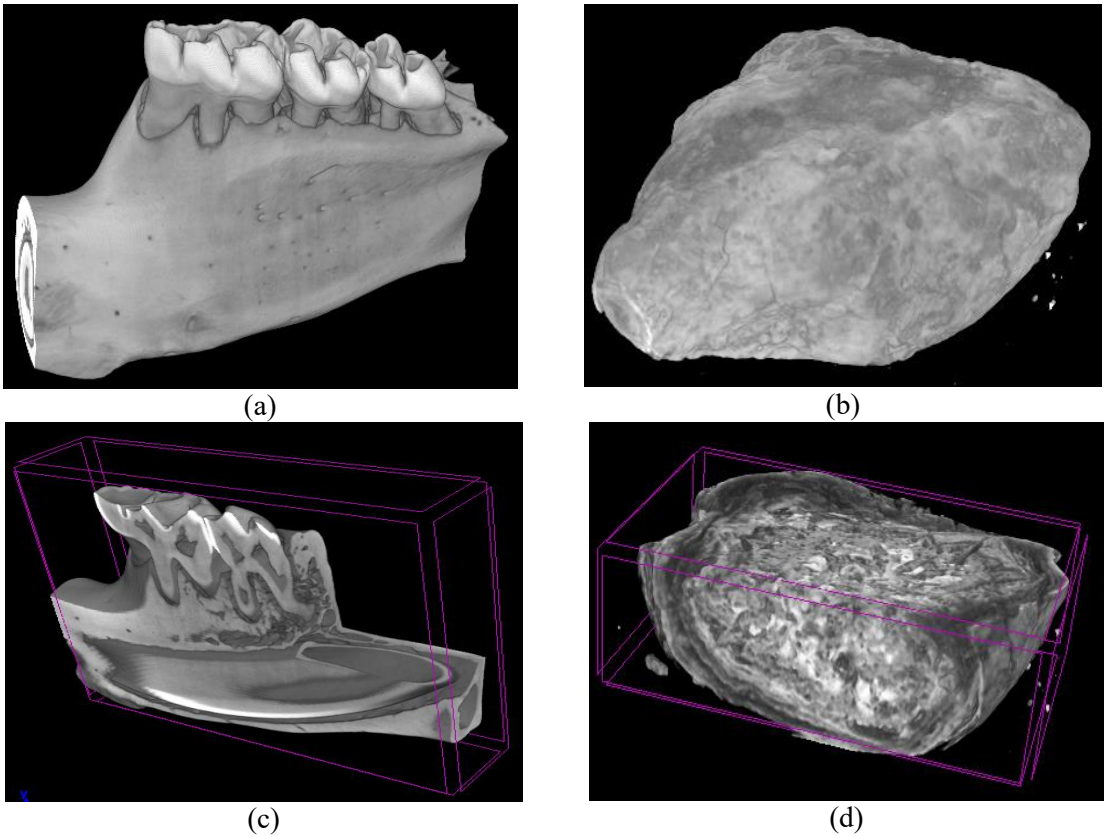

Figure 5. Volumetric renderings of the (a) wistar rat mandible and (b) urinary tract stone; sliced images showing the interior structures of the (a) mandible and (b) stone

Table 3. Calculated morphometric parameters for the two samples

Parameter Name; Symbol; Unit	Sample 1	Sample 2
total VOI volume; TV; mm^3	1.28×10^{11}	$3E\times10^{12}$
object volume; Obj.V; mm^3	8.17×10^{10}	2.44×10^{12}
percent object volume; Obj.V/TV; %	63.74747	81.41616
total VOI surface; TS; mm^2	2.2×10^{8}	1.32×10^{9}
object surface; Obj.S; mm^2	7.12×10^{8}	8.62×10^{9}
object surface/volume ratio; Obj.S/Obj.V; mm^{-1}	1.03×10^{8}	6.8×10^{8}
object surface density; Obj.S/TV; mm^{-1}	0.00872	0.00353
structure thickness; St.Th; mm	0.00556	0.00288
structure separation; St.Sp; mm	-0.00168	-0.00813
total porosity; Po(tot); %	2070.818	12844.73

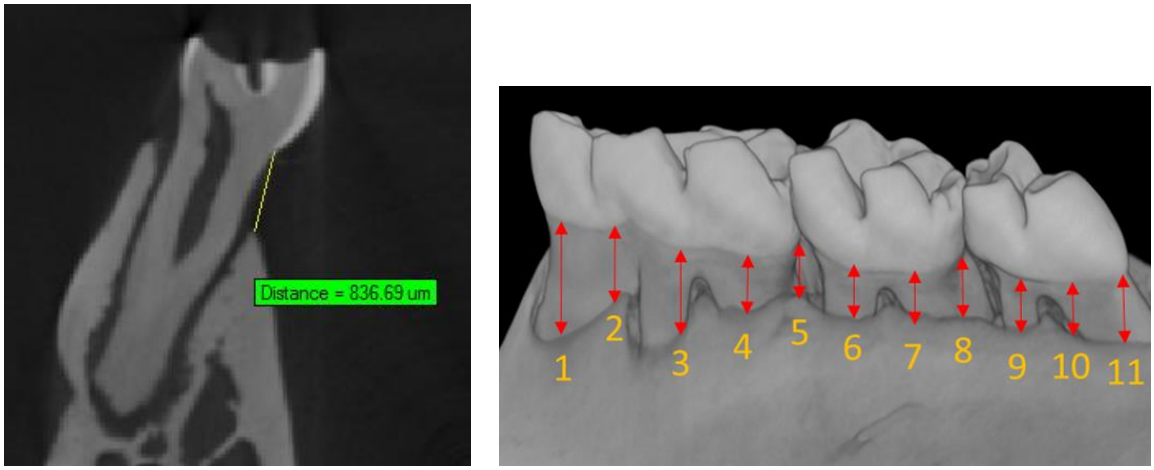

(a) (b)

Point	1	2	3	4	5	6	7	8	9	10	11
Slice #	425	400	375	350	325	300	275	250	225	200	175
Distance (μm)	1260	824	994	557	533	509	436	582	557	533	751

Figure 6. (a) Measuring the distance from the CEJ to the procesus alveolar on a single slice; (b) the points of measurement along the mandible, with corresponding distance measurements presented in the table (bottom)

4. Conclusion

In this paper, we have presented brief analysis of two samples related to dentistry and general medicine. Image acquisition using a Bruker SkyScan 1173 scanner has been described, and the corresponding scanning parameters have also been presented. Examples of possible qualitative analyses, basic primary image processing (VOI selection and thresholding), and several morphometrical variables have also been reported. Additional analyses on both samples have been conducted and reported to demonstrate the possibilities for analysis using digital images obtained from μCT scanning, especially in non-diagnostic *ex vivo* research.

Acknowledgements

This study was partially funded by the government research funding "Riset Desentralisasi DIKTI-ITB (PUPT) 2017" grant from the Ministry of Research-Technology and Higher Education, and Institut Teknologi Bandung research funding "Riset KK-ITB 2017" grant with contract number 108a/11.C01/PL/2017

References

[1] Parsa A, Ibrahim N, Hassan B, Stelt P and Wismeijer D 2015 Bone quality evaluation at dental implant site using multislice CT, micro-CT, and cone beam CT *Clin. Oral. Implants. Res.* **26** e1-7.

[2] Shim J-H, Moon T-S, Yun M-J, Jeon Y-C, Jeong C-M, Cho D-W and Huh J-B 2012 Stimulation of healing within a rabbit calvarial defect by a PCL/PLGA scaffold blended with TCP using solid freeform fabrication technology *J. Mater. Sci. Mater. Med.* **23** 2993-3002.

[3] Pimenta M A, Frasca L C, Lopes R and Rivaldo E 2015 Evaluation of marginal and internal fit of ceramic and metallic crown copings using x-ray microtomography (micro-CT) technology *J. Prosth. Dent.* **114** 223-8.

[4] Vandenberghe B, Luchsinger S, Hostens J, Dhoore E, Jacobs R and Consortium S P 2014 The influence of exposure parameters on jawbone model accuracy using cone beam CT and multislice CT *Dentomaxillofac. Radiol*. **41** 466-74.
[5] Ibrahim N, Parsa A, Hassan B, Stelt P, Aartman I H and Wismeijer D 2014 Accuracy of trabecular bone microstructural measurement at planned dental implant sites using cone-beam CT datasets *Clin. Oral. Implants. Res*. **25** 941-5.
[6] Jung H-D, Yook S-W, Jang T-S, Li Y, Kim H-E and Koh Y-H 2013 Dynamic freeze casting for the production of porous titanium (Ti) scaffolds *Mater. Sci. Eng. C*. **33** 59-63.
[7] Lee J S, Baek S D, Venkatesan J, Bhatnagar I, Chang H K, Kim H T and Kim S-K 2014 In vivo study of chitosan-natural nano hydroxyapatite scaffolds for bone tissue regeneration *Int. J. Biol. Macromol.* **67** 360-6.
[8] Lee J H, Ryu M Y, Baek H-R, Lee K M, Seo J-H, Lee H-K and Ryu H-S 2013 Effects of porous beta-tricalcium phosphate-based ceramics used as an E. coli-derived rhBMP-2 carrier for bone regeneration *J. Mater. Sci.: Mater. Med.* **24** 2117-27.
[9] Tang R, Buckley J M, Fernandez L, Coopey S, Aftreth O, Michaelson J, Saksena M, Lei L, Specht M and Gadd M 2013 Micro-computed tomography (Micro-CT): a novel approach for intraoperative breast cancer specimen imaging *Breast. Cancer. Res. Treat*. **139** 311-6.
[10] Lee J H, Ryu M Y, Baek H-R, Lee K M, Seo J-H and Lee H-K 2013 Fabrication and evaluation of porous beta-tricalcium phosphate/hydroxyapatite (60/40) composite as a bone graft extender using rat calvarial bone defect model. *Scientific. World. J.* **2013** 481789.
[11] Kang S-H, Chung Y-G, Oh I-H, Kim Y-S, Min K-O and Chung J-Y 2014 Bone regeneration potential of allogeneic or autogeneic mesenchymal stem cells loaded onto cancellous bone granules in a rabbit radial defect model *Cell. Tissue. Res*. **355** 81-8.
[12] Atrisandi A, Ramdhani S, Arianto E, Wicaksono N, Mengko T and Latief F 2014 Comparative Study of Water-Logged Meat and Fresh Meat Using Micro-CT. In: The 15th International Conference on Biomedical Engineering: Springer) p. 671-4.
[13] Latief F D E, Dewi D E O, Shari M A B M, Djamal M, Vierdayanti K, Alamsyah I M, Mukti R R, Indrasari W and Islahuddin M 2014 Three-dimensional visualization and characterization of bone structure using reconstructed in-vitro μCT images: A pilot study for bone microarchitecture analysis. In: *AIP Conference Proceedings: AIP* p 418-21.
[14] Sriwayu W O, Haryanto F, Khotimah S N, Latief F D E, Viridi S, Basar K, Iskandar F, Srigutomo W and Gunara B E 2015 Beam hardening and smoothing correction effects on performance of micro-ct SkyScan 1173 for imaging low contrast density materials. In: *AIP Conference Proceedings: AIP Publishing* p 060014.
[15] Fitri L, Asyana V, Ridwan T, Anwary F, Soekersi H, Latief F and Haryanto F 2016 Single energy micro CT SkyScan 1173 for the characterization of urinary stone. In: *J. Phys.: Conference Series: IOP Publishing* p 012074.
[16] Fitri L, Asyana V, Ridwan T, Anwary F, Soekersi H, Latief F and Haryanto F 2016 Dual energy micro CT SkyScan 1173 for the characterization of urinary stone. In: *J. Phys.: Conference Series: IOP Publishing* p 012053.
[17] Latief F D E, Fauzi U and Irayani Z 2013 The Effect of Spatial Resolution on X-Ray μCT Data of Porous Rock. In: *Second International Workshop on Rock Physics*.
[18] Latief F, Irayani Z and Fauzi U 2012 Resolution Dependency of Sandstone's Physical Properties. In: *Annual μCT User Meeting, Belgium*.
[19] Latief F D E, Fauzi U and Feranie S 2012 Digital isolation technique for reconstruction and visualization of cracks in micro-CT images of geothermal reservoir rock *Microsc. Analysis*. 13-7.
[20] Latief F D E, Feranie S, Djamal M, Vierdayanti K, Alamsyah I M, Mukti R R, Indrasari W and Islahuddin M 2014 Three-dimensional visualization and characterization of cracks in geothermal reservoir rock using image analysis of reconstructed μCT images: A preliminary study. In: *AIP Conference Proceedings: AIP* pp 120-3.

[21] Sampurno J, Azwar A, Latief F D E and Srigutomo W 2016 Multifractal characterization of pore size distributions of peat soil *J. Math. Fund. Sci*. **48** 106-14.
[22] Parfitt A M, Drezner M K, Glorieux F H, Kanis J A, Malluche H, Meunier P J, Ott S M and Recker R R 1987 Bone histomorphometry: standardization of nomenclature, symbols, and units: report of the ASBMR histomorphometry nomenclature committee *J. Bone. Miner. Res*. **2** 595-610.
[23] Hildebrand T and Rüegsegger P 1997 A new method for the model-independent assessment of thickness in three-dimensional images *J. Microsc*. **185** 67-75.
[24] Ulrich D, Van Rietbergen B, Laib A and Ruegsegger P 1999 The ability of three-dimensional structural indices to reflect mechanical aspects of trabecular bone *Bone*. **25** 55-60.
[25] Rémy É and Thiel É 2002 Medial axis for chamfer distances: computing look-up tables and neighbourhoods in 2D or 3D *Pattern. Recog. Lett*. **23** 649-61.